Pertanika J. Sci. & Technol. 33 (1): 423 - 440 (2025)

PERTANIKA JOURNALS

SCIENCE & TECHNOLOGY

Journal homepage: http://www.pertanika.upm.edu.my/

Effects of Electron, Gamma and Neutron Irradiation on the Superconducting Properties of $(Bi,Pb)_2Sr_2Ca_2Cu_3O_x$ Bulk Samples

Zaahidah A Mohiju[1], Lay Sheng Ewe[1]*, Roslan Abd-Shukor[2], Weng Kean Yew[3], Hai Song Woon[1] and Abi Muttaqin Jalal Bayar[4]

[1]College of Engineering, Institute of Sustainable Energy (ISE), Universiti Tenaga Nasional, 43000 Kajang, Selangor, Malaysia
[2]Department of Applied Physics, Universiti Kebangsaan Malaysia, 43600 Bangi, Selangor, Malaysia
[3]School of Engineering and Physical Sciences, Heriot-Watt University Malaysia, 62200 Putrajaya, Malaysia
[4]Production Engineering and Metallurgy Department, Malaysian Nuclear Agency, 43000 Selangor, Malaysia

ABSTRACT

In this study, we explored the potential of irradiation techniques to optimize defect concentration and crystal structure in $(Bi,Pb)_2Sr_2Ca_2Cu_3O_{10}$ (Bi-2223) superconductors, aiming to enhance their practicality by potentially improving their critical temperature (T_c) in high magnetic fields. Bi-2223 superconductors have higher T_c and less stringent cooling requirements than low-temperature types, yet enhancing T_c under high magnetic fields is still challenging. The study meticulously compared the electrical properties of Bi-2223 samples in bulk form, subjected individually to electron, gamma, and neutron irradiations, prepared via the conventional solid-state reaction method. Subsequent analyses of structural properties through X-ray diffraction revealed changes in cell lattice parameters, while electrical resistance and AC susceptibility measurements provided insights into the critical temperature. Interestingly, a significant decrease in T_c was observed across all irradiated samples instead of an enhancement, challenging our initial hypothesis. Electron and gamma irradiations led to more homogeneously distributed and less porous defects compared to neutron irradiation, which correlated with the observed decrease in T_c—22.9% for neutron, 16.7% for gamma, and 13.5% for electron irradiation. These results highlight the intricate relationship between the type and distribution of defects induced by different irradiations and their varying impacts on superconductor performance. This study illustrates how defects, based on their characteristics, distinctly affect superconducting properties, emphasizing the complexity of defect interactions in superconductors. Our findings highlight the crucial relationship between irradiation-induced defects and the

ARTICLE INFO

Article history:
Received: 11 March 2024
Accepted: 7 October 2024
Published: 27 January 2025

DOI: https://doi.org/10.47836/pjst.33.1.19

E-mail addresses:
zaahidah.atiqah@yahoo.com (Zaahidah A Mohiju)
laysheng@uniten.edu.my (Lay Sheng Ewe)
ras@ukm.edu.my (Roslan Abd-Shukor)
w.yew@hw.ac.uk (Weng Kean Yew)
hwoon@uniten.edu.my (Hai Song Woon)
abi@nm.gov.my (Abi Muttaqin Jalal Bayar)
*Corresponding author

ISSN: 0128-7680
e-ISSN: 2231-8526

superconducting properties of Bi-2223, suggesting that the impact of T_c reduction on high-temperature superconductor applications needs to be reevaluated.

Keywords: BSCCO-2223, energy, irradiation impact, superconducting properties

INTRODUCTION

There has been a rising interest in conduction-cooled high-temperature superconducting (HTS) magnets for research and industrial purposes, considering their advantages over the traditional low-temperature superconducting magnets requiring liquid helium (Braginski, 2019; Buckel & Kleiner, 2012; Fallah-Arani et al., 2019). This system mainly consists of three phases with the general formula $Bi_2Sr_2Ca_nCu_nO2_{n+4+y}$ where n = 1, 2 and 3, considering the number of CuO_2 layers in the sub-unit cell, respectively. Different methods of preparation, as well as the structural and superconducting properties, have been extensively reported (Amira et al., 2011; Farbod et al., 2016; Hannachi et al., 2018; Salleh et al., 2005; Xu et al., 2010;). Notably, the Bi-2223 phase is preferable due to its highest critical temperature, T_c (~110 K), compared to Bi-2201 (~20 K) and Bi-2212 (~90 K) (Nurbaisyatul et al., 2021). Several techniques have been employed for bulk ceramic superconductor processing, including co-precipitation (Zhang et al., 2021), sol-gel process (Shen et al., 2021), freeze-drying (Jin et al., 2021), and solid-state reaction (Juárez -Lopez et al., 2020).

The solid-state reaction presents a straightforward and cost-effective method. In this study, $Bi_{1.6}Pb_{0.4}Sr_2Ca_2Cu_3O_{10}$ (Bi-2223) powders were produced via the solid-state reaction method. The distinctiveness of Bi-2223 lies in the added Pb, which enhances phase diffusion, accelerates reaction kinetics, creates nucleation centers, and stabilizes the Bi-2223 phase (Anis-ur-Rehman & Mubeen, 2012). In BSCCO systems, lead (Pb) significantly influences the microstructure, phase composition, and superconducting properties. The presence of Pb in the initial mixture promotes the formation of the Bi(Pb)-2223 phase. However, achieving a pure Bi(Pb)-2223 phase is nearly impossible, as it typically coexists with the Bi(Pb)-2212 phase (Nurbaisyatul et al., 2021). Furthermore, Pb promotes grain growth and improves grain connectivity, leading to an improved transport current density, J_c, especially at low fields with a 5 wt% Pb addition (Wang et al., 2010). Also, it induces lattice dislocations within the grains, enhancing the pinning force. It, in turn, leads to an improvement in the critical current density (J_c) (Camargo-Martínez & Baquero, 2016; Lin et al., 2016; Takahira et al., 2015). High critical temperature in superconductors plays a vital role in specific applications such as MRI machines, particle accelerators, and energy-efficient technologies.

Before the discovery of high-temperature superconductors, the idea of superconducting cables existed, but the challenge of long-distance cooling with liquid helium made practical

applications difficult. The advent of high-temperature superconducting cables, cooled with liquid nitrogen, transformed these ideas into feasible solutions. Significant progress has been made in commercializing DI-BSCCO wires, leading to their use in practical applications such as current leads (Hayashi, 2020).

Artificial defects introduced by energetic particle irradiation can improve the critical current in high-temperature superconductors (HTS). Energetic particles, including light ions like protons, deuterium, helium, heavy ions, and high-energy neutrons, create displacement defects, cascades, and voids. These changes affect the vortex patterns in the superconducting material, enhancing its performance (Rajput et al., 2022). Thus, it is an efficient method to introduce pinning centers—the elastic collisions between the accelerated particles on the bulk's surface yield many defects. In the Bi-Sr-Ca-Cu-O system, the highly mobile oxygen atoms can be displaced from their ideal locations when impacted by the energy from incident neutrons. These oxygen atom movements generate numerous vacancies and interstitial oxygen atoms (Kitô et al., 2001; Zhang et al., 2007).

The ability of neutrons to penetrate the specimen bulk creates uniformly distributed defects, where the energy spectrum of the fast neutrons is broadened by scattering and resembles the high energy part of the neutron spectrum in the TRIGA MARK II research reactor, thereby enabling the irradiation of microscopic specimens for further experimentations (Fischer et al., 2018; Karkin et al., 2009). This research explores the effects of electron, gamma, and neutron irradiation on the superconducting properties and microstructure of Bi-2223 superconductor bulk samples. Also, it seeks to investigate whether irradiation can improve the superconducting properties by increasing the concentration of defects in the microstructure. However, Sakurai et al. (2024) notes that increasing the volume fraction of the amorphous regions can lead to a loss of superconducting properties, which may outweigh the benefits provided by the pinning centers.

Understanding the connection between irradiation and the material's properties is crucial for gaining valuable insights into the underlying mechanisms driving these changes. In previous research, compression tests on samples demonstrated that the mechanical properties of Bi-2212 superconductor ceramics, such as porosity, are influenced by varying doses of electron irradiation (Mohiju et al., 2015). The microstructure of irradiated samples, characterized by higher grain orientation and porosity, leads to weaker interface bonding between superconducting grains. Generally, the strength of these samples diminishes with exposure to irradiation, resulting in deformation. Despite this, the formation of point defects within the microstructure, while increasing, enhances the critical current density and transition temperature of the samples (Bi-2212) (Mohiju et al., 2017). Enhancing high-temperature superconductors (HTS) typically requires increasing the complexity of their material composition and microstructure. It is often achieved by introducing defects called artificial pinning centers (APCs). However, this method can clash with efforts to develop

mature, cost-effective mass-production technologies. Interestingly, a notable technique has shown that using dominant pinning centers can maintain the stability of current commercial production without complicating the superconductor's chemistry (Molodyk et al., 2021). In addition, a higher critical current density indicates better flux pinning properties in the sample with additional metal compounds. Studying Bi-2223 can uncover its mysteries, boost its performance, and better understand how superconductors work.

METHODOLOGY

Samples Fabrication

The Bi-2223 superconductor samples were prepared using the conventional solid-state reaction technique. The desired compound, $Bi_{1.6}Pb_{0.4}Sr_2Ca_2Cu_3O_{10}$, necessitated precise proportions of Bi_2O_3, PbO, $SrCO_3$, $CaCO_3$, and CuO with purity of 99%. The first stage requires mixing Bi_2O_3, PbO, $SrCO_3$, $CaCO_3$, and CuO powders in the proportions needed for the desired composition. The powders were ground, mixed and then heated in a tube furnace at 810°C for 30 h. This step helped to catalyze the formation of the Bi-2223 phase.

The resultant powders, predominantly Bi-2223 phase, were compacted under a pressure of 7 tonnes to form pellets, each measuring 13 mm in diameter and 3 mm in thickness. Replicating the conditions of the original heat treatment, the bulk samples were heated at 850 °C for 48 h. The samples were cooled in the furnace down to room temperature in a controlled manner, enabling the material to solidify and maintain favorable properties. The bulk Bi-2223 samples, including structural, electrical resistance and AC susceptibility, were characterized to evaluate their superconducting attributes and performance.

Irradiation Procedure

The electron irradiation process involved using a 3 MeV beam with a current rating of 10 mA. This procedure was executed utilizing the EPS-3000 electron-beam accelerator. The gamma irradiation was performed at the SINAGAMA Irradiation Plant. This plant employs ionizing energy derived from gamma radiation from a cobalt-60 source. The irradiation operations were performed at the Nuclear Malaysia Agency in Bangi, Selangor, Malaysia. The Bi-2223 superconductor bulk samples were subjected to a cumulative dose of 100 kGray in both the electron and gamma irradiation procedures under an open-air environment. Neutron irradiation was carried out with the aid of the PUSPATI TRIGA MARK II research reactor at the Nuclear Malaysia Agency.

Before irradiation, all the necessary procedures were made, including constructing an aluminum holder for the samples and applying protective coverings using aluminum sheets and boron carbide powder. Forecasts were made to predict the activation of elements after the irradiation process. A neutron flux of 2.0×10^{11} neutrons/($cm^2 \cdot s$) was employed

throughout the irradiation, and the samples underwent a 6-hour exposure. As a result, a total fluence of 4.32×10^{15} neutrons/cm^2 was imparted to the samples, effectively triggering the intended irradiation effects. The introduced defects improve flux pinning at low neutron fluences, increasing the critical currents. However, at a certain defect density, the critical current reaches its maximum and I_c declines upon further irradiation. The ability to engineer a product with a pinning microstructure will face arguments such as the doses or level of exposure that produced the most efficient results, which means the critical current reaches its maximum for different magnetic fields and temperatures. According to Koshelev et al. (2016) the ultimate critical-current optimization can be achieved by the constructive combination of different pinning centers; a natural first step is to determine the best pinning configuration for a relatively simple system with only one type of defects (Koshelev et al., 2016).

As stated in the introduction part, where grain growth helps to improve grain connectivity, Aksenova et al. (1995) also stated that under small doses, there is an increase of weak links on grain boundaries caused both by diffusion of atmosphere oxygen to the grain boundaries and the reaction, improving the conducting properties of the intergranular layers. At high doses of gamma irradiation, the intensive degradation of the ceramic surface layer occurs, caused by interaction with air and subsequent changing of phase composition (Aksenova et al., 1995).

Sample Characterization

A D8 Advanced X-Ray Diffractometer (XRD) has been used to determine all samples' phase and structural parameters. Scanning electron microscopy (SEM) provides detailed information that aids in examining the samples' microstructure. This research used the SEM to gather information regarding external morphology (texture), crystalline structure, and grain orientation. The microstructural analysis was conducted using the Hitachi SU8600 Ultra-High-Resolution scanning electron microscope.

The four-point probing technique was utilized to ascertain electrical resistance, with silver paste as the medium for establishing electrical connections. The experimental arrangement comprised a Keithley 197 Multimeter and a Keithley 220 Current Source. A CTI Cryogenics closed-cycle refrigerator Model 22 and a Lake Shore Cryotronics Model 325 temperature controller were employed to assess electrical resistance with respect to temperature. The constant current used was between 1 mA and 100 mA.

AC susceptibility measurements were carried out to identify the temperature of susceptibility transition, denoted as T_χ. The AC susceptibility (represented as $\chi = \chi' + i\chi''$) was deduced using a susceptometer with the model number REF-1808- ACS manufactured by Cryo Industry. The critical current density at the temperature corresponding to the peak

of χ" (designated as T_P) was computed using the formula $J_c(T_P) = H_a/(l_w)^{1/2}$ where l and w stand for the dimensions of the cross-section of the bar-shaped samples.

RESULTS AND DISCUSSION

X-Ray Diffraction

The XRD patterns in Figure 1 show that all the samples display an orthorhombic crystal structure. Post irradiation, slight variations became apparent in the diffraction angles. The patterns pre- and post-irradiation showed changes in peak locations and intensities. These findings demonstrate alterations in the lattice parameter and confirm a reduction in grain size after irradiation. The irradiated samples exhibit significant distortions in the crystal lattice, particularly noticeable in the Bi–O block, which acts as a charge reservoir. Supporting SEM micrographs offer a more distinct visual representation of the diminished grain size induced by irradiation. Collectively, these results signified that irradiation prompts structural modifications in the material, culminating in changes in peak positions, peak intensities, and grain size. By using the Miller indices formula for an orthorhombic crystal structure, $1/d^2 = h^2/a^2 + k^2/b^2 + l^2/c^2$, where h, k and l are numbers from lattice plane, and d is the distance of spacing value obtained from XRD data, the lattice parameters can be calculated. The lattice parameter is related to the atomic radius of the sample's composition (Wang et al., 2007). The investigation centers on the correlation between minor shifts in parameter values within irradiated samples and the structural distortions that result from the interaction between accelerated particles and the samples during irradiation.

The lattice parameters and volume for all samples, including non-irradiated and irradiated samples exposed to different types of radiation (electron, gamma, and neutron). The lattice parameters and unit cell volume are listed for each sample, which remains orthorhombic after irradiation (Table 1). The non-irradiated sample exhibited lattice parameters of a = 5.389 Å, b = 5.398 Å, and c = 37.643 Å, and volume 1095.03 Å^3. Upon electron irradiation, slight changes were observed in the lattice parameters (a = 5.408 Å, b = 5.413 Å, c = 37.015 Å), leading to a reduced volume of 1083.56 Å^3. Similarly, the neutron-irradiated sample showed minor alterations in lattice parameters (a = 5.327 Å, b = 5.303 Å, c = 38.391 Å) with a volume of 1084.51 Å^3. Interestingly, the gamma-irradiated sample shows more significant changes in lattice parameters (a= 5.823 Å, b = 5.271 Å, c = 38.629 Å), resulting in a larger volume of 1185.64 Å^3 compared to both non-irradiated and electron-irradiated samples. The gamma-irradiated sample exhibits more pronounced changes in the lattice parameters compared to electron and neutron irradiation due to the distinct characteristics of gamma radiation. Gamma radiation, high-energy electromagnetic radiation, possesses greater penetration abilities, allowing it to interact deeply with the atoms within the crystal lattice. It led to a higher probability of inducing structural modifications and, therefore, more substantial effects on the material's lattice parameters.

Gamma radiation's higher energy and penetration capabilities facilitate more profound interactions with the material's crystal lattice, causing atomic displacements, defect formations, radiation-induced stress and phase transitions. The phase transition appears to result from a double-hit process: initially, an ion impact creates oxygen defects; subsequently, a second ion hitting the already damaged impact zone triggers a crystalline-to-crystalline phase transition. However, the X-ray diffraction (XRD) patterns show no evidence of such a phase transition in this research. The consistent peak positions across all samples indicate that the orthorhombic structure is retained despite different types of irradiations. Variations in peak intensities suggest changes in the crystalline phase formation within the orthorhombic phase, which may be attributed to factors such as phase purity, preferred orientation, or the degree of crystallinity. These intensity changes reflect alterations in the distribution and alignment of crystal planes rather than a transition to a new phase. In contrast, electron irradiation has noteworthy penetration depths and induced direct interactions with the atoms in the lattice, resulting in significant changes compared to non-irradiated samples.

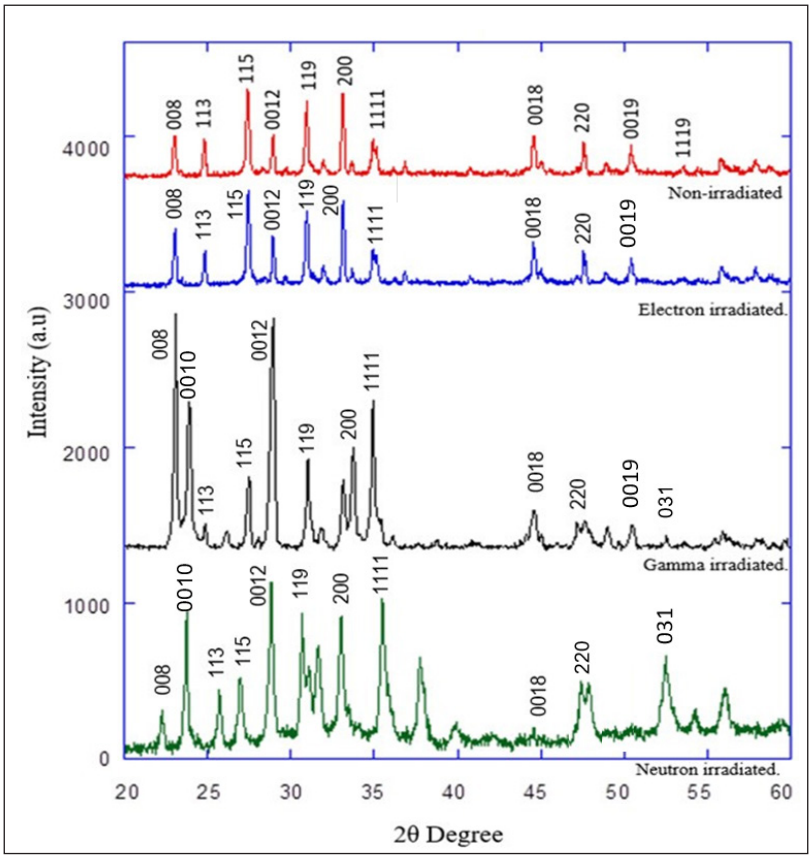

Figure 1. XRD for BSCCO-2223 for non-irradiated and irradiated samples

Table 1
Critical temperature, T_c, peak temperature, T_p, and lattice parameters for all samples

Sample	T_c/K	T_p/K	T_p reduction	Lattice Parameter			Volume
				a/Å	*b*/Å	*c*/Å	*V*/Å^3
Non-irradiated	125	96	-	5.389	5.398	37.643	1095.03
Electron-irradiated	110	83	13.5 %	5.408	5.413	37.015	1083.56
Gamma-irradiated	88	80	16.7 %	5.823	5.271	38.629	1185.64
Neutron-irradiated	100	74	22.9 %	5.327	5.303	38.391	1084.51

In our study of the XRD patterns for BSCCO-2223, we compared the peaks with those identified by the previous researcher, Fallah-Arani et al. (2019). We discovered several unidentified peaks at specific angles in all samples, particularly those exposed to electron, gamma, and neutron irradiation. These unidentified peaks suggest the possible development of new secondary phases within the BSCCO-2223 structure.

Furthermore, the XRD patterns for non-irradiated, electron-irradiated, gamma-irradiated and neutron-irradiated samples show significant differences in peak intensities at various angles (2θ) due to the distinct effects of each irradiation type on the crystalline structure. Gamma-irradiated samples exhibit higher intensities for the 008 and 0012 planes, likely due to reorientation or redistribution of crystalline planes and induced defects. Neutron-irradiated samples show intense peaks at the 0012 and 1111 planes as neutron irradiation penetrates deeper, causing displacement damage and strain within the lattice. Both types of irradiations introduce defects, alter crystallite size, and induce strain, affecting peak intensities. Despite the visible changes in crystallite size, the crystallite structure can remain the same. Non-irradiated samples show baseline intensities, reflecting the original structure, while electron-irradiated samples exhibit moderate changes, indicating less penetration.

Electrical Resistance and AC Susceptibility

Figures 2(a)–(d) illustrate non-irradiated and irradiated samples' electrical resistance versus temperature profiles. Each graph is marked with the respective critical temperature (T_c). In the case of the non-irradiated bulk sample, T_c was 125 K. Interestingly, the irradiated samples exhibit a gradual reduction in T_c, with values of 110 K, 100 K, and 88 K for electron, neutron, and gamma irradiation, respectively. This decline in critical temperature is a noteworthy observation. The neutron-irradiated sample exhibits the most significant alterations in T_c compared to the electron-irradiated and gamma-irradiated samples, as shown in Table 1.

Figure 3 displays the AC susceptibility ($\chi = \chi' + i\chi''$) measurements for both irradiated and non-irradiated samples. In these measurements, a noticeable shift or peak in the graph emerges precisely at the critical temperature, marking the transition from the ordinary state to the superconducting state. The graph comprises two distinct segments: the real part χ',

which signifies diamagnetic behavior, and the imaginary part χ", illustrating the efficacy of the flux pinning centers and the interconnection among grains. The peak observed in χ" graph, is denoted as T_p. By examining the χ" graph, we can deduce AC losses by comparing the values of these two peaks. The higher temperature peak represents intrinsic losses and reveals the intragranular current density (J_c−intra). The applied magnetic field influences the positions of both loss peaks in χ".

Our experimental setup utilized a low magnetic field, which prevented the H_{ac} (alternating field) from piercing the grains. Consequently, a higher temperature peak was absent. However, the magnetic field was sufficient to penetrate within the grains and reveal the intergranular loss peak (T_p). By maintaining an applied magnetic field (5 Oe), the strength of flux pinning was assessed by analyzing the degree of shifting and the width of the intergranular loss peak.

The AC susceptibility measurements were crucial in understanding the samples' superconducting behavior. The values of χ' and χ" were analyzed to determine various aspects, including transition temperatures, intrinsic and coupling losses, and the strength of flux pinning based on the shifting and width of the intergranular loss peak.

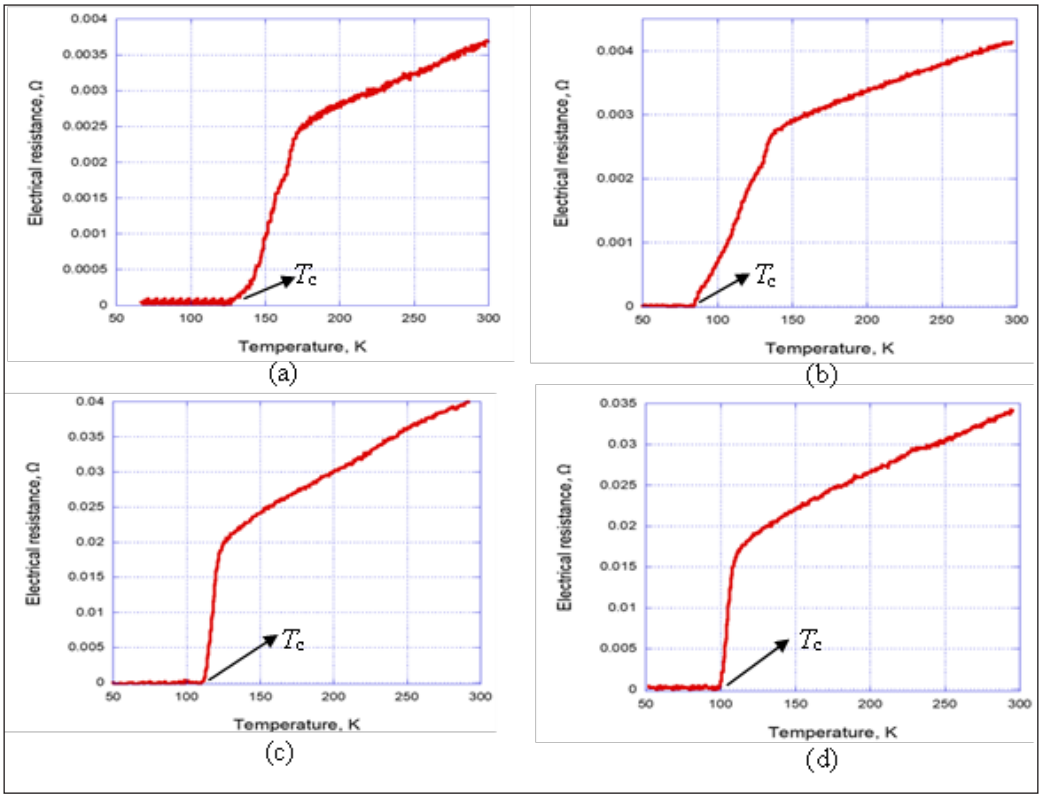

Figure 2. Electrical Resistance *vs* Temperature for (a) non-irradiated bulk sample. (b) Gamma-irradiated bulk sample. (c) Electron-irradiated bulk sample and (d) Neutron-irradiated bulk sample

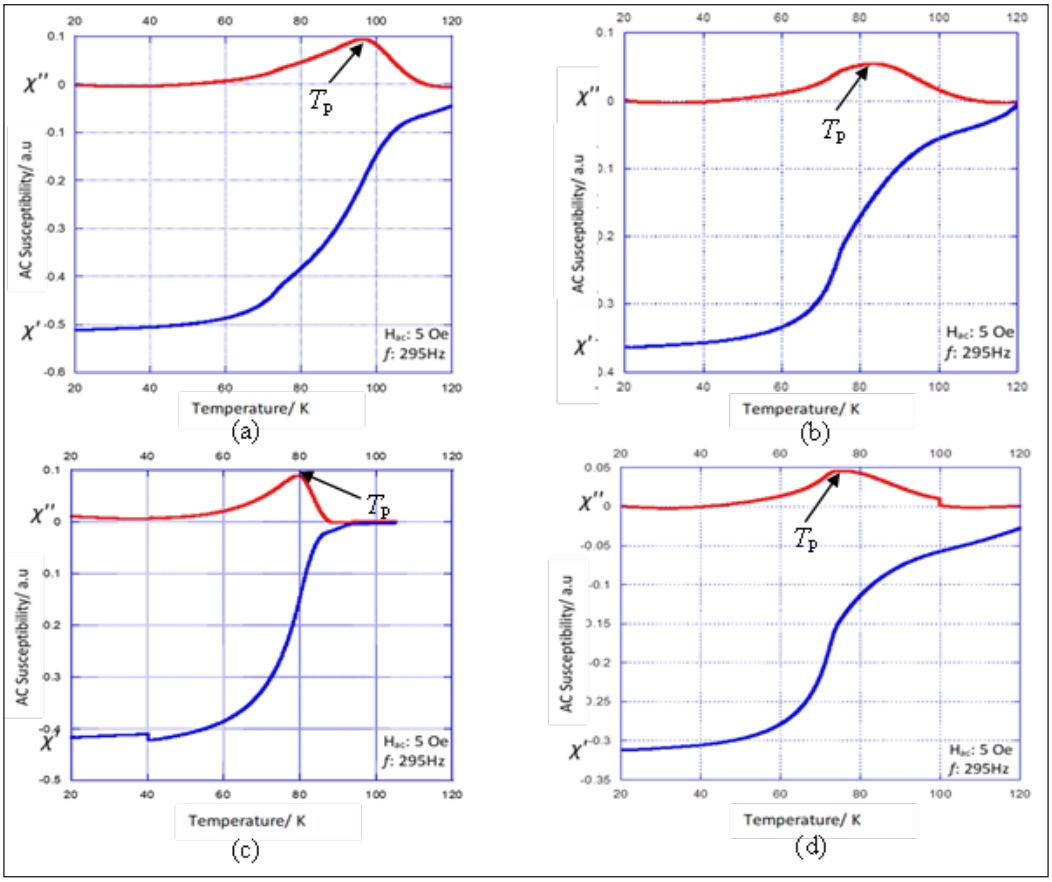

Figure 3. AC susceptibility of Bi-2223 for (a) non-irradiated sample, (b) electron-irradiated sample, (c) gamma-irradiated sample, (d) neutron-irradiated sample

Table 1 displays the critical temperature (T_c) and peak temperature (T_p) values for Bi-2223 superconductor bulk samples exposed to different irradiation conditions. In the non-irradiated sample, T_c registers at 112 K, while T_p, marking the onset of irreversibility in superconducting behavior, appears at 96 K. The shift in T_c for electrical resistance and T_p for AC susceptibility measurements is primarily due to the concentration of defects created by the irradiation. At the same time, $T_{c\text{-onset}}$ and $T_{c\text{-offset}}$ represent different stages of the superconducting transition, with $T_{c\text{-onset}}$ indicating the initial formation of superconducting regions and $T_{c\text{-offset}}$ signifying the complete transition to the superconducting state. Electron irradiation reduces T_c to 110 K and significantly lowers T_p to 83 K, marking a 13.5% decrease compared to the non-irradiated sample, showing defect introduction disrupting superconducting behavior. Similarly, gamma irradiation decreases T_c (to 88 K) and T_p (to 80 K), resulting in a 16.7% reduction compared to the non-irradiated sample, indicating defect-induced impact on superconducting properties.

Neutron irradiation lowers T_c to 100 K, with T_p dropping notably to 74 K, representing a 22.9% decrease compared to the non-irradiated sample, highlighting neutron irradiation's substantial disruption of superconducting behavior. The differences in the initial and complete superconducting transition temperatures (Tc-onset and Tc-offset) across the samples can be explained by the varying energy levels of the irradiation sources. Higher-energy irradiations, like neutron irradiation, create larger defects that disrupt the superconducting state more extensively. It leads to a broader range of superconducting transitions, affecting various material parts. In contrast, lower-energy irradiation, such as electron irradiation, generates smaller defects that cause more consistent superconducting transitions across the material. This variation in irradiation energy affects how defects are introduced, which influences both the beginning and the end of the superconducting transition, explaining the differences seen in $T_{c\text{-onset}}$ and $T_{c\text{-offset}}$.

The reduction in T_c and T_p observed after irradiation indicates that defects introduced by irradiation act as pinning centers for magnetic flux lines, which can enhance the material's ability to carry superconducting currents. This phenomenon is desirable in many practical applications requiring high critical currents and magnetic field tolerances. Therefore, while irradiation may lower the absolute critical temperature, it can simultaneously improve the material's performance under certain conditions, making it more suitable for practical use in specific applications.

Scanning Electron Microscopy (SEM) Micrographs

The samples' micrographs provide further insights into the underlying mechanisms (Figures 4 to 8). The observations indicate changes in both the grain size and the grain orientation.

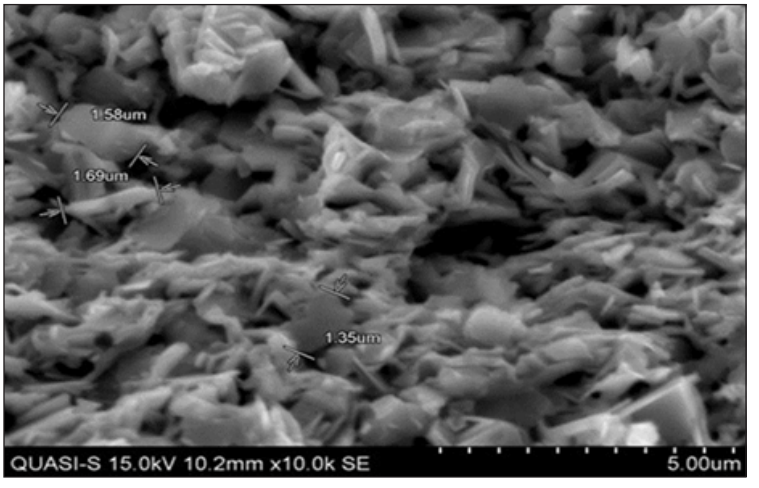

Figure 4. The grain size of non-irradiated Bi-2223

The micrographs showed a non-uniform phase distribution on the samples' surface. Some areas exhibit a layered structure, characteristic of the crystal structure of the Bi-2223 system. The samples also display a porous nature with grain sizes between 1.35 μm and 1.69 μm.

The presence of plate-like grains, typical of Bi-based high-temperature superconductors, was observed in the samples. The lamellar structure, associated with high critical temperature superconductors, can be seen in many grains. However, following irradiation, the grain size slightly decreased, and porosity increased (Figures 5 to 8). The grains exhibited a random distribution, indicating anisotropic grain orientation and poor interconnection between the grains. The Hall-Petch relation also expressed the influence of the grain size on mechanical properties such as ductile-brittle transition and tensile and hardness of polycrystalline materials (Armstrong, 1970; Hansen, 2004). Additionally, as the particles crystallize and bond together, the cavities between the particle grains become more numerous because the sintering process involves the elimination of porosity and the densification of the material. As the particles bond, the material becomes more compact, reducing the overall volume and increasing the density. This reduction in volume can create additional space (black regions) between the particle grains, resulting in cavities or voids (Imaduddin et al., 2023).

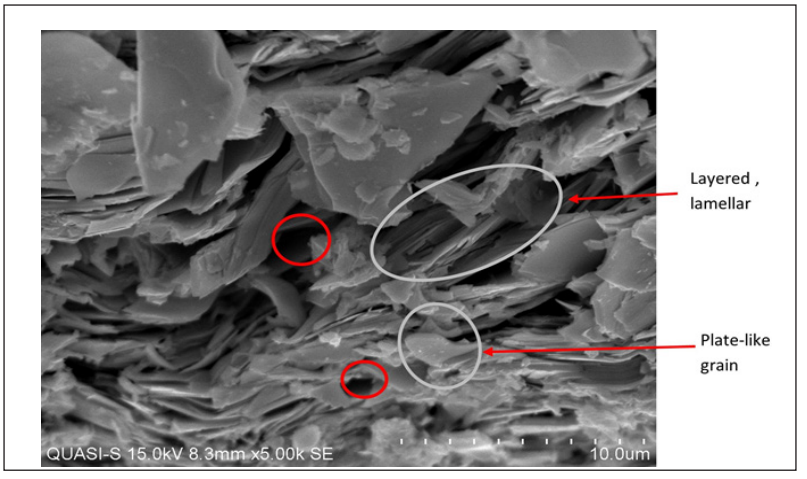

Figure 5. Microstructure of non-irradiated Bi-2223. The black regions circled in red represent randomly distributed grains within the matrix structure, indicating a weaker linkage between the grains

In Figures 5 to 8, the black regions circled in red represent randomly distributed grains within the matrix structure, indicating a weaker linkage between the grains. It is expected that after irradiation, the Bi-2223 compound will exhibit a higher density of grain boundaries due to the increased concentration of defects caused by accelerated particles. As particles crystallize and bond during sintering, the material becomes denser as air pockets are removed and the particles are compacted. This densification reduces the overall volume

of the material, minimizing the spaces or voids between the particle grains. This reduction in volume can create extra space (appearing as black regions) between the grains, forming cavities or voids. Similar in size to coherence length, these defects act as pinning centers due to their distribution and link to local variations in critical temperature. This arrangement boosts the creation of effective pinning centers while slightly decreasing the average size of the Bi-2223 crystallites (Al-Khawaja, 2006). This enhanced the formation of effective pinning centers while slightly reducing the average size of the Bi-2223 crystallites.

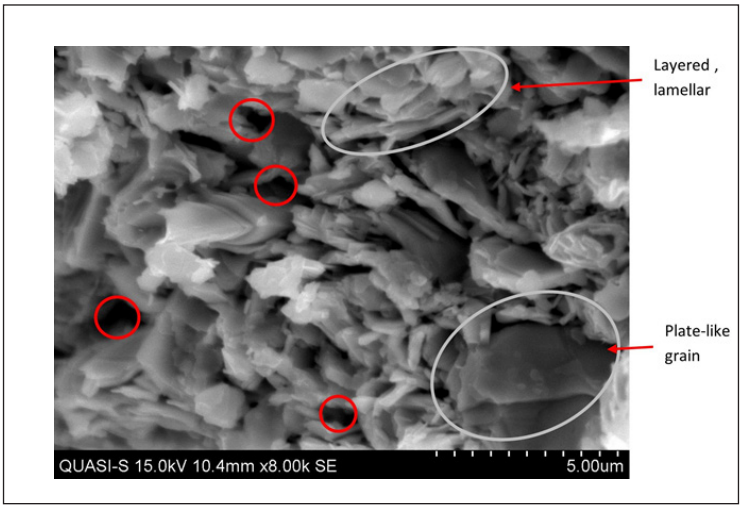

Figure 6. Microstructure of electron-irradiated Bi-2223. The black regions circled in red represent randomly distributed grains within the matrix structure, indicating a weaker linkage between the grains

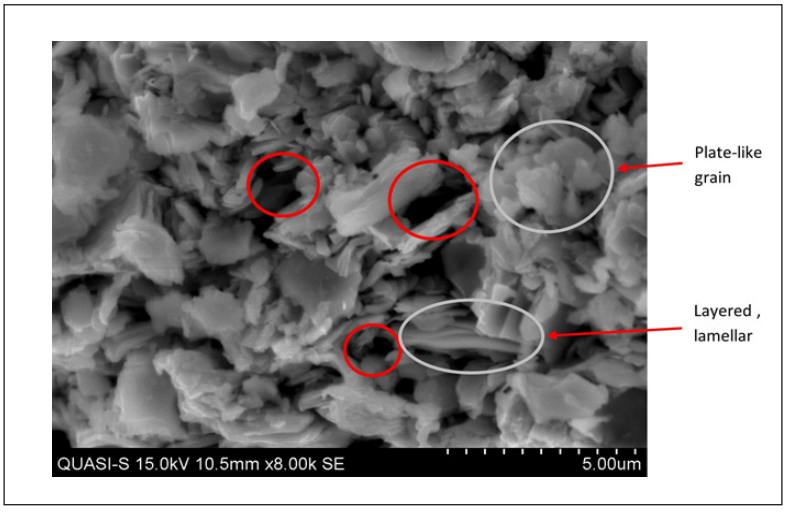

Figure 7. Microstructure of gamma-irradiated Bi-2223. The black regions circled in red represent randomly distributed grains within the matrix structure, indicating a weaker linkage between the grains

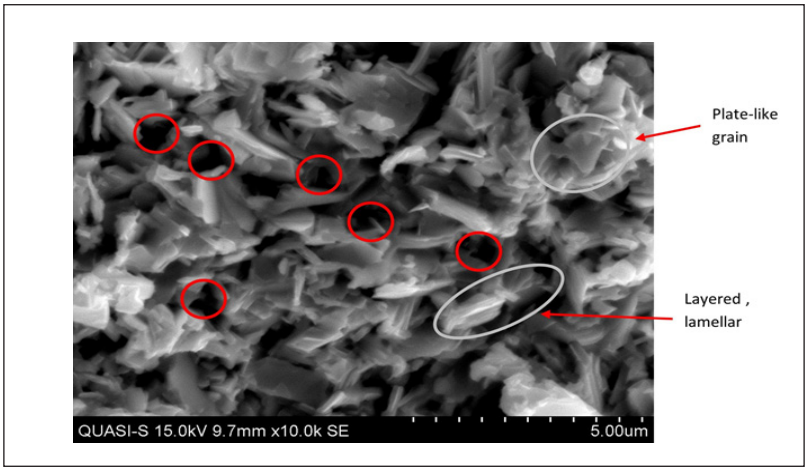

Figure 8. Microstructure of neutron-irradiated Bi-2223. The black regions circled in red represent randomly distributed grains within the matrix structure, indicating a weaker linkage between the grains

The micrographs showed that the non-irradiated samples have the densest layering structure. This robust layering signals a well-organized and densely packed distribution of grains within the non-irradiated sample. In contrast, the samples subjected to electron irradiation reveal a slightly less dense layering structure than the non-irradiated counterpart. It suggests that electron irradiation triggered minor alterations in the grain configuration, leading to a slight disarrangement in the dense layering, which is evident in the non-irradiated sample. On the other hand, the sample exposed to gamma irradiation exhibits a more significant reduction in the layered structure's density compared to both non-irradiated and electron-irradiated samples.

This finding suggests that gamma irradiation has a more potent effect on the layered structure, resulting in a larger degree of disruption and a less compact arrangement of grains. The sample exposed to neutron irradiation displays the least dense layered structure among all the samples. Neutron irradiation seems to exert the most pronounced impact on the layered microstructure, culminating in a more spread-out and less orderly grain arrangement. The Figures 5 to 8 distinctly illustrate a trend concerning the layering structure's density across the samples. The non-irradiated sample manifests the highest density, followed by the electron-irradiated, gamma-irradiated, and ultimately the neutron-irradiated sample.

CONCLUSION

This study reveals that electrons, gamma, and neutron irradiations reduce the critical temperature (T_c) and peak temperature (T_p) of Bi-2223 superconductors. Among these, neutron irradiation causes the most significant decrease in T_p by 22.9%, highlighting its

effectiveness in introducing microstructural defects. These defects serve as pinning centers, disrupting superconducting capabilities more than other irradiation types. Consequently, neutron irradiation is identified as the most impactful method for modifying Bi-2223's superconducting properties.

However, the choice of irradiation technique should be tailored to specific application needs, as neutron irradiation's aggressive effects might not always be desirable. Future research should optimize the balance between defect introduction and superconducting performance, particularly under high magnetic fields. Rigorous statistical analysis is essential to validate the irradiation effects and ensure that superconductor development is based on reliable data. This approach will help modify superconductor properties for specific applications, advancing the field of superconductivity.

ACKNOWLEDGMENT

The authors acknowledge Universiti Tenaga Nasional for the Bold Grant 2023, project code J510050962, for providing funding resources that contributed to the research results reported within this paper.

REFERENCES

Aksenova, T. I., Berdauletov, A. K., & Daukeev, D. K. (1995). Effect of gamma irradiation on physical and chemical processes in YBaCuO. *Radiation Physics and Chemistry, 46*(4-6), 533-536. https://doi.org/10.1016/0969-806X(95)00211-F

Al-Khawaja, U., Benkraouda, M., Obaidat, I. M., & Alneaimi, S. (2006). Numerical simulations on the role of the defect size on the critical current in high-temperature superconductors. *Physica C: Superconductivity and its applications*, *442*(1), 1-8. https://doi.org/10.1016/j.physc.2006.03.134

Amira, A., Boudjadja, Y., Saoudel, A., Varilci, A., Akdogan, M., Terzioglu, C., & Mosbah, M. F. (2011). Effect of doping by low content of yttrium at Ca and Sr sites of Bi (Pb)-2212 superconducting ceramics. *Physica B: Condensed Matter*, *406*(4), 1022-1027. https://doi.org/10.1016/j.physb.2010.12.052

Anis-ur-Rehman, M., & Mubeen, M. (2012). Synthesis and enhancement of current density in cerium doped Bi (Pb) Sr (Ba)-2 2 2 3 high Tc superconductor. *Synthetic Metals*, *162*(19-20), 1769-1774. https://doi.org/10.1016/j.synthmet.2012.03.006

Armstrong, R. W. (1970). The influence of polycrystal grain size on several mechanical properties of materials. *Metallurgical Transactions*, *1*(5), 1169–1176. https://doi.org/10.1007/BF02900227

Braginski, A. I. (2019). Superconductor electronics: Status and outlook. *Journal of Superconductivity and Novel Magnetism*, *32*(1), 23–44. https://doi.org/10.1007/s10948-018-4884-4

Buckel, W., & Kleiner, R. (2012). *Supraleitung: Grundlagen und anwendungen* (7th ed.). Wiley.

Camargo-Martínez, J. A., & Baquero, R. (2016). Effects of Pb doping on structural and electronic properties of Bi2Sr2Ca2Cu3O10. *Physica C: Superconductivity and Its Applications*, *521*, 22–28. https://doi.org/10.1016/j.physc.2015.12.006

Fallah-Arani, H., Baghshahi, S., Sedghi, A., & Riahi-Noori, N. (2019). Enhancement in the performance of BSCCO (Bi-2223) superconductor with functionalized TiO2 nanorod additive. *Ceramics International, 45*(17), 21878-21886. https://doi.org/10.1016/j.ceramint.2019.07.198

Farbod, M., Rafati, Z., & Shoushtari, M. Z. (2016). Optimization of parameters for the synthesis of Y2Cu2O5 nanoparticles by Taguchi method and comparison of their magnetic and optical properties with their bulk counterpart. *Journal of Magnetism and Magnetic Materials*, *407*, 266-271. https://doi.org/10.1016/j.jmmm.2016.01.069

Fischer, D. X., Prokopec, R., Emhofer, J., & Eisterer, M. (2018). The effect of fast neutron irradiation on the superconducting properties of REBCO coated conductors with and without artificial pinning centers. *Superconductor Science and Technology, 31*(4), Article 044006. https://doi.org/10.1088/1361-6668/aaadf2

Hannachi, E., Slimani, Y., Azzouz, F. B., & Ekicibil, A. H. M. E. T. (2018). Higher intra-granular and inter-granular performances of YBCO superconductor with TiO2 nano-sized particles addition. *Ceramics International, 44*(15), 18836-18843. https://doi.org/10.1016/j.ceramint.2018.07.118

Hansen, N. (2004). Hall–Petch relation and boundary strengthening. *Scripta materialia, 51*(8), 801-806. https://doi.org/10.1016/j.scriptamat.2004.06.002

Hayashi, K. (2020). Commercialization of Bi-2223 superconducting wires and their applications. *Sei Technical Review*, *91*, 68-74.

Imaduddin, A., Herbirowo, S., Nugraha, H., Hendrik, H., Aisatun, A., Giovanni, A. R., Effendi, M., Sari, K., Pramono, A. W., & Yuwono, A. H. (2023). Evolution of morphological, crystal structure, and electrical properties of Ba-Pb-Bi-O superconducting materials. *South African Journal of Chemical Engineering, 46*(1), 112-121. https://doi.org/10.1016/j.sajce.2023.07.014

Jin, L. H., Liu, G. Q., Xu, X. Y., Jiao, G. F., Zheng, H. L., Hao, Q. B., Zhang, S. N., Li, C. S., & Zhang, P. X. (2021). Evolution of precursor powders prepared by oxalate freeze drying towards high performance Bi-2212 wires. *Ceramics International*, *47*(3), 3299-3305. https://doi.org/10.1016/j.ceramint.2020.09.170

Juárez-Lopez, J. M., Guillén-Cervantes, A., Quiñones-Galván, J. G., Nieto-Zepeda, K. E., Zelaya-Angel, O., Santos-Cruz, J., Diaz-Valdes, E., Contreras-Puente, G., & Moure-Flores, D. F. (2020). Structural and morphological characterization of $YBa_2Cu_3O_7$-x films deposited by screen printing from $YBa_2Cu_3O_6$. 962 superconductor in bulk. *Materials Research Express*, *7*(9), Article 096001. https://doi.org/10.1088/2053-1591/abadd0

Karkin, A. E., Werner, J., Behr, G., & Goshchitskii, B. N. (2009). Neutron-irradiation effects in polycrystalline LaFeAsO0.9F0.1 superconductors. *Physical Review B—Condensed Matter and Materials Physics, 80*(17), Article 174512. https://doi.org/10.1103/PhysRevB.80.174512

Kitô, H., Iyo, A., Tokumoto, M., Okayasu, S., & Ihara, H. (2001). Effect of the neutron irradiation of the high temperature superconductor $(Cu,C)Ba_2Ca_{n-1}Cu_nO_{2n+4-\delta}$ (n=3, 4 and 5). *Physica C: Superconductivity*, *357*, 234–236. https://doi.org/10.1016/S0921-4534(01)00217-9

Koshelev, A. E., Sadovskyy, I. A., Phillips, C. L., & Glatz, A. (2016). Optimization of vortex pinning by nanoparticles using simulations of the time-dependent Ginzburg-Landau model. *Physical Review B*, *93*(6), Article 060508. https://doi.org/10.1103/PhysRevB.93.060508

Lin, H., Yao, C., Zhang, X., Zhang, H., Zhang, Q., Wang, D., Dong, C., & Ma, Y. (2016). Effect of metal (Zn/In/Pb) additions on the microstructures and superconducting properties of $Sr_{1-x}K_xFe_2As_2$ tapes. *Scripta Materialia*, *112*, 128–131. https://doi.org/10.1016/j.scriptamat.2015.09.031

Mohiju, Z. A., Hamid, N. A., & Abdullah, Y. (2017) Enhancement of flux pinning properties in nanosized MgO added Bi-2212 superconductor through neutron irradiation. *AIP Conference Proceedings, 1799*(1), Article 040004. https://doi.org/10.1063/1.4972928

Mohiju, Z. A., Hamid, N. A., Abdullah, Y., & Kannan, V. (2015). Effect of electron irradiation exposure on phase formation, microstructure and mechanical strength of $Bi_2Sr_2CaCu_2O_8$ superconductor prepared via co-precipitation method. *AIP Conference Proceedings, 1659*(1), Article 040006. https://doi.org/10.1063/1.4916866

Molodyk, A., Samoilenkov, S., Markelov, A., Degtyarenko, P., Lee, S., Petrykin, V., Gaifullin, M., Mankevich, A., Vaivilov, A., Sorbom, B., Cheng, J., Garberg, S., Kesler, L., Hartwig, Z., Gavrilkin, S., Tsvetkov, A., Okada, T., Awaji, S., Abraimov, D., … & Vasiliev, A. (2021). Development and large volume production of extremely high current density $YBa_2Cu_3O_7$ superconducting wires for fusion. *Scientific reports*, *11*(1), Article 2084. https://doi.org/10.1038/s41598-021-81559-z

Nurbaisyatul, E. S., Azhan, H., Ibrahim, N., & Saipuddin, S. F. (2021). Structural and superconducting properties of low-density Bi (Pb)-2223 superconductor: Effect of Eu_2O_3 nanoparticles addition. *Cryogenics, 119*, Article 103353. https://doi.org/10.1016/j.cryogenics.2021.103353

Rajput, M., Swami, H. L., Kumar, R., Bano, A., Vala, S., Abhangi, M., Prasad, U., Kumar, R., & Srinivasan, R. (2022). Deuterium ion irradiation impact on the current-carrying capacity of DI-BSCCO superconducting tape. *Nuclear Engineering and Technology*, *54*(7), 2586-2591. https://doi.org/10.1016/j.net.2022.02.008

Sakurai, K., Yamashita, A., Mizuguchi, Y., Yabuuchi, K., & Oono-Hori, N. (2024). Irradiation effects on copper oxide superconductors including high-entropy REBCO (HE-REBCO). *Nuclear Materials and Energy*, *40*, Article 101709. https://doi.org/10.1016/j.nme.2024.101709

Salleh, F. M., Yahya, A. K., Imad, H., & Jumali, M. H. (2005). Synthesis and formation of TlSr1212 superconductors from coprecipitated oxalate precursors. *Physica C: Superconductivity, 426*, 319-324. https://doi.org/10.1016/j.physc.2005.02.043

Shen, M., Zhao, G., Lei, L., Ji, H., & Ren, P. (2021). The intrinsic Josephson effect of Bi-2212 superconducting thin films prepared by sol-gel method. *Ceramics International*, *47*(24), 35067-35072. https://doi.org/10.1016/j.ceramint.2021.09.048

Takahira, S., Ichino, Y., & Yoshida, Y. (2015). Fabrication of high Jc (Bi, Pb) 2223 thin films by PLD and post-annealing process. *Physics Procedia*, *65*, 153-156. https://doi.org/10.1016/j.phpro.2015.05.089

Wang, L., Qi, Y., Zhang, Z., Wang, D., Zhang, X., Gao, Z., Yao, C., & Ma, Y. (2010). Influence of Pb addition on the superconducting properties of polycrystalline $Sr_{0.6}K_{0.4}Fe_2As_2$. *Superconductor Science and Technology*, *23*(5), Article 054010. https://doi.org/10.1088/0953-2048/23/5/054010

Wang, T., Chen, L. Q., & Liu, Z. K. (2007). Lattice parameters and local lattice distortions in fcc-Ni solutions. *Metallurgical and Materials Transactions, A*, *38*, 562-569. https://doi.org/10.1007/s11661-007-9091-z

Zhang, H., Li, G., Zhou, T. F., Liu, Y., Li, X. G., & Chen, Y. (2007). Effects of neutron irradiation on superconducting properties of $GdBa_2Cu_3O_7$-δ single domain superconductor. *Chinese Journal of Chemical Physics*, *20*(3), 324. https://doi.org/10.1088/1674-0068/20/03/324-328

Zhang, S., Ma, X., Shao, B., Cui, L., Liu, G., Zheng, H., Liu, X., Feng, J., Li, C., & Zhang, P. (2021). Fabrication of multifilamentary powder in tube superconducting tapes of Bi-2223 with Sr deficient starting composition. *Cryogenics*, *114*, Article 103245. https://doi.org/10.1016/j.cryogenics.2020.103245